All-Hydrocarbon-Ligated Superatomic Gold/Aluminum Clusters

Ivan Antsiburov, Max Schutz, Raphael Bühler, Maximilian Muhr, Johannes Stephan, Christian Gemel, Wilhelm Klein, Samia Kahlal, Jean-Yves Saillard, Roland A. Fischer

All-Hydrocarbon Ligated Superatomic Gold/Aluminium Clusters.

Ivan Antsiburov[‡ a,b], *Max Schütz*[‡ a,b], *Raphael Bühler*[a,b], *Maximilian Muhr*[a,b], *Johannes Stephan* [a,b] *Christian Gemel*[a,b], *Wilhelm Klein* [a,b], *Samia Kahlal*[c], *Jean-Yves Saillard**[c] *and Roland A. Fischer**[a,b]

[a] Technical University of Munich, Department of Chemistry and Catalysis Research Center, Chair of Inorganic and Metal-Organic Chemistry, Lichtenbergstr. 4, 85748 Garching, Germany. E-mail: roland.fischer@tum.de

[b] Univ Rennes, CNRS, ISCR-UMR 6226, F-35000 Rennes, France. E-mail: jean-yves.saillard@univ-rennes1.fr

[‡] *Ivan Antsiburov* and *Max Schütz* contributed equally.

KEYWORDS gold clusters, bimetallic cluster synthesis, DFT calculations, cluster formation, superatoms

ABSTRACT

Key strategies in cluster synthesis include the use of modulating agents (e.g. coordinating substrates). We studied the influence of various phosphines exhibiting different steric and electronic properties on the reduction of the Au(I) precursor to Au(0)-clusters. We report a synthesis of the bimetallic clusters $[Au_6(AlCp^*)_6] = [Au_6Al_6](Cp^*)_6$ (**1**) and $[HAu_7(AlCp^*)_6] = [HAu_7Al_6](Cp^*)_6$ (**2**) (Cp* = pentamethylcyclopentadiene) using Au(I) precursors and AlCp*. The cluster $[Au_2(AlCp^*)_5] = [Au_2Al_5](Cp^*)_5$ (**3**) was isolated and identified as an intermediate species in the reaction to **1** and **2**. The processes of cluster growth and degradation were investigated by *in situ* ^{1}H-NMR and LIFDI-MS techniques. The structures of **1** and **2** were established by DFT geometry optimization. These octahedral clusters can both be described as closed-shell 18-electron superatoms.

INTRODUCTION

Gold clusters are known for more than 50 years and are among the most thoroughly studied metal clusters.[1-5] The investigation of their structures, electronic properties and reactivity profiles contributed a lot to the general understanding of cluster chemistry and the nature of metal-metal bonding.[6-8] The physical and chemical properties of a cluster are determined by its ligand shell and the precise number of metal atoms in the core.[9] The most widely studied are gold clusters, bearing phosphines or thiolate ligands, such as the famous *Schmid cluster* $[Au_{55}](PPh_3)_{12}Cl_6$ or the thiolate stabilized $Au_{25}(SR)_{18}$.[2, 10, 11] Such clusters are typically obtained by the reduction of Au(I) or Au(III) precursors, e.g. $[AuCl_4]^-$ or $(R_3P)AuCl$, in the presence of stabilizing and cluster growth controlling phosphine or thiolate ligands. However the precise size-selectivity (atomicity, nuclearity) of the cluster synthesis is most often impossible.[10] Common reducing agents for the Au-precursors used in the synthesis of gold clusters and nanoparticles are borohydrides, carboxylic acids or polyols, amongst many others.[12]

Usually, these reducing agents serve as a source of electrons, without providing additional stabilizing interactions with the formed product clusters. A different approach, combining a reducing and cluster stabilizing agent in one molecule are for example low valent group 13 organometallic compounds ECp* (E = Al, Ga).[13-16] The reaction of AlCp* with {CuMes} under various conditions, for example, leads to the formation of clusters $[Cu_7Al_6](Cp^*)_6$, $[HCu_7Al_6](Cp^*)_6$, $[Cu_8Al_6](Cp^*)_6$ and $[Cu_{43}Al_{12}](Cp^*)_{12}$. In these reactions Cu(I) is reduced to Cu(0) by AlCp*, $AlMes_3$ and $AlMes_2Cp^*$ arising as oxidized side products. In a similar manner, the reaction of AlCp* with $\{(PPh_3)CuH\}_6$ gives the cluster $[H_4Cu_6Al_6](Cp^*)_6$. In this case, also the elimination of H_2 is observed as a parallel pathway for the reduction of Cu(I). The notation of cluster formulas that we prefer highlight the hydrocarbon protected bimetallic core structure $[H_xAu_aAl_b](Cp^*)_b$, rather than specifying the selective binding of Cp* to Al, which is highlighted by the notation $[H_xAu_a(AlCp^*)_b]$.

In this work we describe the synthetic access to the three new gold-aluminium clusters $[Au_6Al_6](Cp^*)_6$ (**1**), $[HAu_7Al_6](Cp^*)_6$ (**2**), and $[Au_2Al_5](Cp^*)_5$ (**3**). Heteronuclear gold clusters with late transition metals (e.g. Pd, Pt) were studied intensively in the past and show promising reactivities such as the activation of H_2.[17] In contrary, intermetallic gold clusters with p-block metals received considerably less attention with only a few examples known in the literature.[18-20]

The initial reaction of the precursors ^{i}DippAuH (^{i}Dipp = 2,3-dihydro-1,3-bis(2,6-diisopropylphenyl)-1H-imidazol-2-ylidene) and AlCp* (Cp* = η^5-C_5Me_5) leads to a library of various Au/Al clusters of different nuclearity. Inspired by similar concepts in nanoparticle synthesis,[21-24] we recently showed that the product distribution in the synthesis of related Ni/Ga and Ni/Al clusters can be narrowed down to singular products by using alkynes as additives during synthesis (coordination modulation).[25] In the present case, phosphines were chosen as adequate additives, due to their ability to stabilize the Au(0) centers.[26]

The geometric and electronic structures of the larger clusters $[Au_6Al_6](Cp^*)_6$ (**1**) and $[HAu_7Al_6](Cp^*)_6$ (**2**) were investigated by calculations on the DFT level of theory, revealing the bonding situation in **1** and **2** related to the corresponding Cu/Al superatomic clusters.

EXPERIMENTAL SECTION

General

All experiments were conducted using standard Schlenk and glovebox techniques under an atmosphere of purified argon. All solvents were carefully dried over molecular sieves (water content < 5 ppm) and degassed prior to their use. The starting compounds AlCp* and ^{i}DippAuH (^{i}Dipp = 1,3-bis(2,6-diisopropylphenyl)imidazol-2-ylidene). were prepared according to literature methods.[27, 28] For **1**, and the co-crystallizate **1**/**2** no meaningful data for the elemental analysis (C, H, Au, Al) could be obtained. Satisfying elemental analysis data of pure isolated compound **2** and **3** were obtained. However, based on the spectroscopic data of pure **2**, the assignments of LIFDI MS[29] and ^{1}H NMR data for **1** and **1/2** were possible. NMR spectra were recorded on a Bruker Avance III AV400US (^{1}H, 400 MHz; ^{13}C 101 MHz). Chemical shifts are described in ppm relative to tetramethylsilane (TMS) and referenced to the solvent residual signals. FT-IR spectra were measured with an ATR setup using Bruker Alpha FTIR spectrometer under an inert gas atmosphere in a glove-box. UV-Vis spectra were measured in toluene under inert atmosphere with an Agilent Carry 60 spectrometer.

Synthesis of $[Au_6Al_6](Cp^*)_6$ (1)

Samples of $(PPh_3)AuCp^*$ (305 mg, 538 µmol, 1.0 eq.) and AlCp* (125 mg, 807 µmol, 1.5 eq) were heated in 30 mL of toluene at 75 °C for 2 h. The hot, orange reaction solution was filtered and concentrated *in vacuo* to 12 mL. The resulting solution was stored at – 32 °C for seven days and at – 86 °C for four days. The formed, brown crystalline precipitate was filtered off, washed with hexane (3×5 mL) and with pentane (4×2 mL) and dried *in vacuo* giving pure **1** (52.4 mg, 24.3 µmol, 27%). This cluster is pyrophore.

^{1}H-NMR (400 MHz, Benzene-d_6) δ 1.94 (s, 90H).

^{13}C NMR (126 MHz, Benzene-d_6) δ 115.21 (s, quaternary *C* (Cp*)), 13.00 (s, *C*H_3).

IR (ATR, 298 K): ν [cm^{-1}] = 2907 (m), 2849 (m), 2361 (w), 2340 (w), 1425 (s), 1370 (s), 795 (s), 727 (s), 422 (vs) cm^{-1}.

UV-Vis (298 K, toluene): 513 nm (broad), 385 – 400 nm (shoulder, strong), 360 – 380 nm (shoulder, small), 307 nm (sharp).

LIFDI-MS: m/z = m/z = 2155 ($[Au_6Al_6](Cp^*)_6]^+$).

No satisfying elemental analysis data of **1** could be obtained due to the high sensitivity of the cluster.

Synthesis of $[HAu_7Al_6](Cp^*)_6$ (2)

Samples of ^{i}DippAuH (150 mg, 256 µmol, 1.0 eq.), AlCp* (31 mg, 192 µmol, 0.75 eq) and PPh_3 (201 mg, 767 µmol, 3.0 eq.) were heated in 15 mL of toluene at 75 °C for 3 h. The hot, dark-red reaction solution was filtered and stored at – 32 °C for seven days. The formed dark crystalline precipitate was filtered off, washed with pentane (2×5 mL) then with THF (3×1 mL) and again with pentane (3×1 mL) and dried in a glovebox giving the pure cluster **2** (22 mg, 9.3µmol, 26%).

^{1}H-NMR (298 K, 400 MHz, C_6D_6): 1.99 (s (broad), 90H, C*H*$_3$ (Cp*)).

^{13}C-NMR (298 K, 500 MHz, cryo-probe, C_6D_6): 115.5 (s, quaternary *C* (Cp*)), 12.9 (s, *C*H_3).

IR (ATR, 298 K): ν [cm^{-1}] = 3552 (w), 3483 (w), 2964 (w), 2902, 2850, 1753, 1452 (shoulder), 1421, 1371, 1310 (b, i), 1050 (w), 1027 (w), 801, 729, 694, 587, 451 (i).

UV-Vis (298 K, toluene): 514 nm (broad), 480 nm (very weak), 415 - 463 nm (shoulder, strong), 298 nm (sharp).

LIFDI-MS: m/z = 2351 ($[Au_7Al_6](Cp^*)_6]^+$).

Elemental analysis [%]: Calculated for $Au_7Al_6C_{60}H_{90}$: C: 30.64, H: 3.86, Al: 6.88, Au: 58.62; found: C: 29.95, H : 3.88, Al: 6.73, Au: 58.41.

Synthesis of $[DAu_7Al_6](Cp^*)_6$ (2D)

Samples of ^{i}DippAuD (125 mg, 213 µmol, 1.0 eq.), AlCp* (26 mg, 160 µmol, 0.75 eq) and PPh_3 (168 mg, 638 µmol, 3.0 eq.) were heated in 15 mL of toluene at 75 °C for 3 h. The hot, dark-red reaction solution was filtered and stored at – 32 °C for seven days. The formed dark crystalline precipitate was filtered off, washed with pentane (2×5 mL) then with THF (3×1 mL) and again

with pentane (3×1 mL) and dried in a glovebox giving the pure cluster **2D** (15 mg, 6.4µmol, 24%).

^{1}H-NMR (298 K, 400 MHz, C_6D_6): 1.99 (s (broad), 90H, C*H*$_3$ (Cp*)).

IR (ATR, 298 K): ν [cm^{-1}] = 3552 (w), 3483 (w), 2964 (w), 2902, 2850, 1452 (shoulder), 1421, 1371, 1310 (b, i), 1260 (i), 1050 (w), 1027 (w), 801, 729, 694, 587, 451 (i).

LIFDI-MS: m/z = 2351 ($[Au_7Al_6](Cp^*)_6]^+$).

Synthesis of $[H_{0-1}Au_{6/7}Al_6](Cp^*)_6$ (1/2)

Samples of ^{i}DippAuH (150 mg, 0.256 mmol, 1.0 eq.) and AlCp* (41.56 mg, 0.256 mmol 1.0 eq.) were heated in 15 mL of toluene at 75 °C for 3 h. After a short time, some gas evolution was observed. The dark-red reaction solution was filtered and stored at -30 °C for several weeks. The formed dark crystalline precipitate was isolated by means of filtration and washed with *n*-hexane (3 x 0.1 ml) and benzene (3 x 0.1 ml) resulting in pure **1/2** (10 mg, 4.4 µmol, 11%).

^{1}H-NMR (298 K, 400 MHz, C_6D_6): 1.99 (s (broad), 90H, C*H*$_3$ (Cp*) of **2**), 1.94 (s (broad), 90H, C*H*$_3$ (Cp*) of **1**).

^{13}C-NMR (298 K, 500 MHz, cryo-probe, C_6D_6): 12.99 (s, *C*H$_3$ (Cp*) of **1**), 115.2 (s, quaternary *C* (Cp*) of **1**), 115.5 (s, quaternary *C* (Cp*) of **2**).

IR (ATR, 298 K): ν [cm^{-1}] = 2959 (w), 2904, 2845, 1756 (w), 1595, 1411, 1358, 1325, 1264, 1230, 1201, 1158 – 915 (b, i), 889, 809, 781, 742, 685, 638, 546, 426.

UV-Vis (298 K, toluene): 513 nm (broad), 478 nm (very weak), 440 nm (shoulder, weak), 309 nm (sharp).

LIFDI-MS: m/z = 2155 ($[Au_6Al_6](Cp^*)_6]^+$), 2351 ($[Au_7Al_6](Cp^*)_6]^+$).

Synthesis of $[Au_2Al_5](Cp^*)_5$ (3)

Samples of ^{i}DippAuH (100 mg, 170 µmol 1.0 eq.) and AlCp* (69 mg, 426 µmol, 2.5 eq.) were heated in 5 mL of toluene to 75 °C for 20 h. The hot, dark-brown reaction solution was filtered and stored at – 32 °C for two weeks. The formed dark needles were filtered off, washed with

pentane (5×0.1 mL) then dissolved in 2.5 mL hexane at 70 °C and stored at – 32 °C for 6 d. Crystals were isolated by decantation, washed with cold pentane (3×0.2 mL) and dried in a glovebox giving the pure cluster **3** (18.5 mg, 15.4 μmol, 18%).

^{1}H-NMR (298 K, 400 MHz, C_6D_6): 2.19 (s (very broad), 45H, bridging AlCp*), 1.85 (s (very broad), 30H, terminal AlCp*).

^{13}C-NMR (298 K, 500 MHz, cryo-probe, C_7D_8): 114.19 (s, quaternary C), 13.65 (s, -*C*H_3), 10.23 (s, -*C*H_3).

LIFDI-MS: m/z = 1203 ([**3**-H]$^{+}$).

IR (ATR, 298 K): ν [cm^{-1}] = 2964 (w), 2900, 2848, 2712 (w), 1487 (w), 1417, 1369, 1176 (w), 1019, 799, 578, 455 (i).

UV-Vis (298 K, toluene): 498-536 nm (weak, broad), 478 nm (broad), 406 nm (very broad), 331 nm (sharp).

Elemental analysis [%]: Calculated for $Au_2Al_5C_{50}H_{75}$: C: 49.84, H: 6.27, Al: 11.20, Au: 32.69; found: C: 49.00, H: 6.22, Al: 10.87, Au: 32.51.

Computational details

Density Functional Theory (DFT) calculations[30] were carried out with the use of the Amsterdam Density Functional code (ADF2019) [31-33] incorporating scalar relativistic corrections via the ZORA Hamiltonian,[34] and with the addition of Grimme's D3(BJ) empirical corrections[35] in order to take into account dispersion effects. The all-electron triple-ξ Slater basis set plus two polarization functions (STO-TZ2P),[36] was used, together with the Becke-Perdew (BP86)[37, 38] exchange-correlation functional. All the optimized structures were confirmed as true minima on their potential energy surface by analytical vibration frequency calculations. Natural atomic orbital (NAO) populations and Wiberg bond indices were computed with the natural bond orbital NBO6.0 program[39] implemented in the ADF2019 package. The NMR chemical shifts were computed according to the gauge-independent atomic orbitals (GIAO) method.[40] Owing to the too long demand of CPU time required by the ADF2019 code for these clusters, the

Gaussian 16 package[41] was used for calculating the UV-visible electronic transitions by means of time-dependent DFT (TD-DFT) calculations. The PBE0 hybrid functional[42, 43] was chosen for the sake of accuracy, together with the Def2TZVP basis set.[44, 45] The UV-visible spectra were simulated from the computed TD-DFT transitions and their oscillator strengths, each transition being associated with a Gaussian function of half-height width equal to 1500 cm^{-1}

Results and Discussion

Synthesis and spectroscopic characterization of $[Au_6Al_6](Cp^*)_6$ (1)

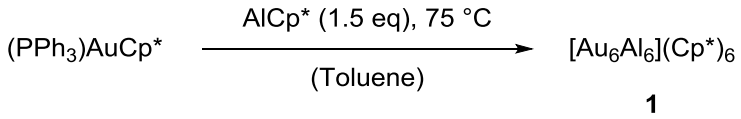

Scheme 1: Synthesis of the $[Au_6Al_6](Cp^*)_6$ (**1**).

The cluster $[Au_6Al_6](Cp^*)_6$ (**1**) was prepared by reaction of $(PPh_3)AuCp^*$ with AlCp* in 27 % yield (Scheme 1). The preparative purity of isolated **1** is confirmed by ^{1}H-NMR analysis in benzene-d_6, exhibiting only one peak at 1.94 ppm as the only signal besides very small impurities of HCp* (see Figure S1). The ^{13}C-NMR spectrum shows the quaternary carbon signal of the Cp* ligands of **1** at 115.21 ppm and the signal of methyl groups at 13.00 ppm (see Figure S2). LIFDI-MS analysis of isolated **1** reveals the presence of **1** together with trace amounts of **2**. Observed molecular peaks and fragments include (see Figure S9): $[Au_6Al_6](Cp^*)_5^+$ (m/z 2019.79), $\{[Au_6Al_6](Cp^*)_7 - H\}^+$ (m/z 2289.20) and $\{[Au_7Al_6](Cp^*)_7 - H\}^+$ (m/z 2486.17). ATR-IR spectrum of **1** shows the expected bands of C-H, C-C and Al-Cp* stretching as well as C-H bending (Figure S11). Two signals at 2361 and 2340 cm^{-1} could not be assigned. The bands in this range are typical for CO_2, but no CO_2 has been present inside the glovebox (Ar inert gas) where the sample was prepared and measured. The wavenumbers of these two signals are significantly higher than the value of 1753 cm^{-1} observed for the ν(Au-H) stretching vibration of $[HAu_7Al_6](Cp^*)_6$ (*vide infra*). The UV-Vis spectrum of isolated **1** in toluene shows a prominent absorption band at 496 nm – 540 nm (maximum: 513 nm), a strong shoulder at 385 – 400 nm as well as a weak shoulder at 360 – 380 nm (see Figure S13).

Synthesis and characterization of $[HAu_7Al_6](Cp^*)_6$ (2).

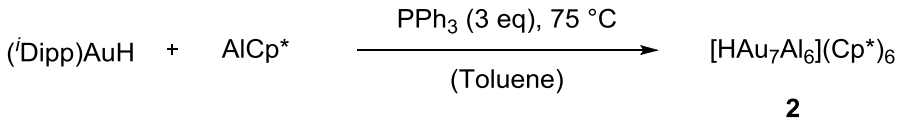

Scheme 2: Synthesis of the $[HAu_7Al_6](Cp^*)_6$ (**2**).

The cluster $[HAu_7Al_6](Cp^*)_6$ (**2**) was prepared by reaction of ^{i}DippAuH with AlCp* in presence of a high excess of PPh_3 with 26 % yield (Scheme 2).

The reaction outcome of ^{i}DippAuH and AlCp* in presence of PR_3 (10 eq.) exhibiting different electronic properties was studied by *in situ* ^{1}H-NMR spectroscopy (see Figure S33 – 46). In the most cases with mono- (PPh_3, P(*p*-Tol)$_3$, P(anis)$_3$, PEt_3, P(*n*-Oct)$_3$, P(*i*-Pr)$_3$) and bidentate (dppbz, dppe) the selective formation of **2** is observed. The selectivity towards **2** was lower in the presence of P(4-FC_6H_4)$_3$ and a small amount of **1** is observed. The presence of very bulky PCy_3 or P(*o*-Tol)$_3$ lead to a mixture **1**/**2**, i.e. the same reaction outcome as in the absence of any additive. Presence of small, strongly -σ-donating phosphines PMe_3 or depe lead to precipitation of elemental gold. Usage of phosphites ($P(OPh)_3$ or $P(OMe)_3$) leads to decomposition under P-O bond cleavage and the phosphinidene ^{i}Dipp=PH arises as a side product. Notably AlCp* as well as ^{i}DippAuH alone are unreactive towards $P(OR)_3$.

The reduction of Au(I) in ^{i}DippAuH to Au(0) in **2** happens through reductive elimination of H_2 or by reduction with AlCp*, which is confirmed by *in situ* NMR measurements (Figure S30 and Figure S33).

The purity of **2** is confirmed by ^{1}H-NMR analysis in benzene-d_6, exhibiting only one peak at 1.99 ppm as the only signal besides very small impurities of PPh_3 and co-crystallized toluene (see Figure S4). The signal of hydride could not be detected neither at room temperature nor at -80 °C. The ^{13}C-NMR spectrum shows the quaternary carbon signal of the Cp* ligands of **2** at 115.50 pm (see Figure S5). The signal of -*C*H_3 carbon atoms at 12.91 ppm could be only observed in DEPT 135° experiment (see Figure S6). Likewise, the LIFDI-MS spectrum of isolated **2** shows the molecular ion peak of **2** as the only signal attributable to a cluster species (see Figure S10). The IR spectrum of **2** (see Figure S11) exhibits the characteristic C-H stretching (2790 – 3012 cm^{-1}), C-H deformation (1178 – 1335 cm^{-1}; 729 cm^{-1}) and C-C

stretching (1380 – 1497 cm^{-1}) modes of the Cp* ligand are again identified in the spectrum in addition to the Al-Cp* stretching frequency at 445 cm^{-1}. A characteristic ν(Au-H) stretching vibration is discernible at 1720 – 1780 cm^{-1}. The band exhibits maximum absorption at 1753 cm^{-1}, as well as two shoulders at 1735 cm^{-1} and 1770 cm^{-1}. This value is very similar to IR data of $[AuH_4]^-$ (1676.4 cm^{-1}, 1678.8 cm^{-1}) and $[H_2AuH_3]$ (1651.5 cm^{-1}, 1666.8 cm^{-1}) obtained in matrix isolation experiments, whereas the frequencies observed for [AuH] (2226.6 cm^{-1}) and also for ^{i}DippAuH (1976 cm^{-1}) are found at higher wavenumbers.[28, 46] This assignment was confirmed through the preparation of the corresponding deuteride cluster (**2D**) from the ^{i}DippAuD (86% deuterium according to ^{1}H-NMR). Indeed, the band at 1753 cm^{-1} is almost vanished and a new intense band at 1260 cm^{-1} arises (Figure S12). This value is in a good agreement with the computed one 1236 cm^{-1} (Figure S61). The UV-Vis spectrum of isolated **2** in toluene shows the prominent absorption band at 494 nm – 540 nm (maximum: 514 nm) and the minor band at 480 nm, the shoulder at 415-463 nm (see Figure S13). Single crystals of **2** are obtained upon crystallization from toluene at – 35 °C. SC-XRD analysis of these crystals leads to a highly disordered structure, the data obtained upon refinement are not sufficiently accurate for a detailed discussion of structural parameters. However, the overall structural motive is confirmed by SC-XRD data analysis. It consists of a disordered Au_7 core, which adopts an approximate cube-shaped geometry with one missing vertex. This unit is embedded in an octahedral Al_6 shell (see Figure S58).

Computational DFT investigation

In order to shed some light on the structure, bonding and stability of clusters **1** and **2**, we investigated them through DFT calculations at the BP86/TZ2P-D3 level (see Computational Details). The experimental, disordered solid-state structure of **2**, somewhat reminds that of the copper-aluminium clusters $[HCu_7Al_6](Cp^*)_6$ and $[Cu_8Al_6](Cp^*)_6$, which are disordered too.[15] In any case, the structures derived from analysis of X-ray diffraction data suggest an M_n (M = Au, Cu) core embedded within a distorted $(AlCp^*)_6$ octahedron and DFT calculations confirmed this type of arrangement for $[HCu_7Al_6](Cp^*)_6$ and $[Cu_8Al_6](Cp^*)_6$.[15] When looking for structures of this type in the case of **2**, four low-energy isomers were found, lying within a range of 5 kcal/mol (Figure S59). The most stable, both in total (E) and free (G) energies is shown in Figure 2 and selected computed data are provided in Table 1. Its structure can be viewed as a quite distorted

Au cube having a missing vertex and lying within an $(AlCp^*)_6$ octahedron. The other energy minima exhibit more or less similar features. The hydride occupies a terminal position at a gold atom (Au-H = 1.664 Å). The corresponding computed Au-H stretching frequency (1745 cm^{-1}) is close to the experimental value, as well as the computed ^{13}C and ^{1}H NMR chemical shifts (Figure S59). Two other low-energy isomers also meet these criteria (Figure S59). Unfortunately, neither the ^{1}H chemical shift of the hydride of **2** (computed value: 8.8 ppm) nor ^{2}H of the deuteride of **2D** could not be experimentally recorded, likely due to fluxionality. As its isoelectronic relative $[HCu_7Al_6](Cp^*)_6$, the shape of cluster **2** is enough pseudo-spherical for being described as an 18-electron superatom[8, 47] of $1S^2\ 1P^6\ 1D^{10}$ configuration, with 1 and 2 electron(s) provided by each Au(0) and Al(I) atom, respectively, with the exception of the Au atom described as Au(I), linked to the terminal hydride (H^-) , which is formally a 0-electron supplier ligand. Consistently, the five highest Kohn-Sham orbitals are of large 6s(Au) and 3s/3p(Al) character and resemble, although somehow dented, the pure 1D orbitals of a quasi-spherical superatom (Figure S60).

Three low-energy isomers (Figure S59) were found for **1**, of which the two lowest are almost degenerate in total energy and differ by less than 4 kcal/mol in free energy. They can all be viewed as deriving from a substantially distorted Au cube having two missing vertices and lying within an (also distorted) $(AlCp^*)_6$ octahedron. The isomer of lowest energy is shown in Figure 2 and selected computed data are provided in Table 1. It is also possible to view it as an 18-electron superatom with its five highest occupied orbitals constituting the 1D set (Figure S60).

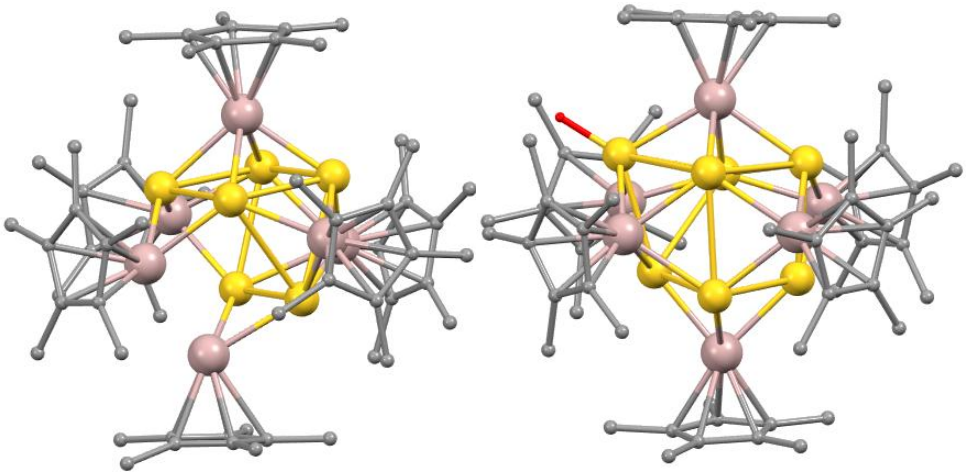

Figure 2: DFT-optimized geometries of the lowest energy isomers of $[Au_6Al_6](Cp^*)_6$ (**1**) and $[HAu_7Al_6](Cp^*)_6$ (**2**).

Clusters **1** and **2** show similar bonding features (Table 1), with strong Au-Al bonding and weaker Au-Au interactions. The Au-H WBI indicates substantial covalency. The Au and Al NBO charges reflect their actual oxidation states and the rather moderate negative charge of the hydride is consistent with the Au-H covalency.

TD-DFT calculations on the lowest energy isomers of **1** and **2** were performed with the PBE0 hybrid functional and the Def2SVP basis set with solvent effect (see Computational Details). The simulated spectra are in sufficient agreement with the experimental data (Figure S62 and S63).

In the case of **1**, **t**he three bands of lowest energy have maxima at 521, 442 and 377 nm The first one corresponds to a HOMO-1 → LUMO-1 transition, thus being of 1D → 1F nature. The second one (mainly HOMO → LUMO+3 and HOMO-2 → LUMO+2) and the third one (mainly HOMO-1 → LUMO+5, HOMO-1 → LUMO+6 and HOMO-2 → L+6) are also of 1D → 1F nature. The intense band of higher energy peaking at 313 nm corresponds to π*(Cp*) → 1F, *i.e.* LMCT, transitions.

A comment about isomerism should be made at this point of the discussion. Although we found several low-energy minima in the cases of both **1** and **2**, we cannot certify that their number is not larger than that we found. In fact, all the computed isomers can be described as approximately spherical 18-electron superatoms, and it is likely that their shape is soft enough to allow generation of several structures of the same type in the reaction medium, with possible

interconversion between them. Such a feature is consistent with the highly disordered nature of the experimental structural data obtained by the X-ray diffraction study of **2** (Figure S58).

Table 1: Selected computed data for the lowest energy isomers of **1** and **2**. WBI = Wiberg bond index (in brackets).

Compound		**1**	**2**
HOMO-LUMO gap (eV)		1.96	1.40
Distances (Å) [WBI]	Au-Au (av. and range)	2.898 [0.025] 2.762-2.995	2.910 [0.019] 2.792-3.073
	Al-Au (av. and range)	2.574 [0.322] 2.501-2.667	2.567 [0.316] 2.484-2.671
	Au-H	-	1.664 [0.436]
NBO charges	Au (av. and range)	0.00 (-0.02)-(+0.03)	+0.07 (-0.03)-(+0.24)
	Al (av. and range)	+0.57 (+0.50)-(+0.63)	+0.55 (+0.49)-(+0.71)
	H		-0.38

The parentage between the 18-electron superatoms $[HAu_7Al_6](Cp^*)_6$ and $[HCu_7Al_6](Cp^*)_6$[11], both made of a $(Au/Cu)_7$ core embedded within an $(AlCp^*)_6$ octahedron, suggests the possibility of existence of $[Au_8Al_6](Cp^*)_6$, isoelectronic to the isolated $[Cu_8Al_6](Cp^*)_6$.[11] The latter is a 20-electron species ($1S^2\ 1P^6\ 1D^{10}\ 1S^2$ configuration) featuring a $Cu_4@Cu_4$ tetracapped tetrahedron (contracted cube) encapsulated within an $(AlCp^*)_6$ octahedron. Our search for a stable closed-shell $[Au_8Al_6](Cp^*)_6$ species ended up with a structure exhibiting a quite regular (not contracted) Au_8 cube encapsulated within an $(AlCp^*)_6$ octahedron and for which the unique favored closed-shell electron count is 18, corresponding to the dication $\{[Au_8Al_6](Cp^*)_6\}^{2+}$ (Figure S59d). The difference between the "Cu_8Al_6" and "Au_8Al_6" species is their different availabilities of the superatomic 2S orbital. It is the HOMO in the Cu/Al case, but only the LUMO+4 in the Au/Al case, the LUMO to LUMO+3 being part of the 1F set. The non-availability of the 2S orbital in the Au species is consistent with the lower compacity of its Au_8 core. Calculations on the isoelectronic hypothetical dihydride $[H_2Au_8Al_6](Cp^*)_6$ provided similar results as for its

$[Au_8Al_6](Cp^*)_6]^{2+}$ dicationic parent, thus suggesting the possibility for these two 18-electron species to be observed.

Synthesis and characterization of $[Au_2Al_5](Cp^*)_5$ (3)

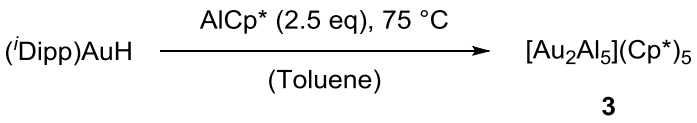

Scheme 3: Synthesis of the $[Au_2Al_5](Cp^*)_5$ (**3**).

The reaction of ^{i}DippAuH with excess of AlCp* (2.5 eq.) in toluene after prolonged reaction times (18 h) leads to the formation of the cluster $[Au_2Al_5](Cp^*)_5$ (**3**) (Scheme 3).

The preparative purity of **3** is confirmed by ^{1}H-NMR analysis in benzene-d_6, exhibiting two broad signals at 2.21 and 1.86 ppm with integral ratio 3:2, assigned to the bridging and terminal AlCp* ligands respectively (see Figure S14). The ^{13}C-NMR spectrum of **3** in toluene-d_8 (see Figure S15) shows the two signals of the -*C*H$_3$ groups of the terminal and bridging AlCp* moieties at 13.65 ppm and 10.23 ppm. However, only one signal at 114.19 ppm is observed for the quaternary carbon atoms. The elemental analysis yields satisfying data. LIFDI-MS analysis of the isolated product shows the molecular ion peak **3**-H$^+$ as weak signal at m/z = 1203.4 (see Figure S16) besides several fragment species of **3**, such as $[AuAl_2](Cp^*)_2^+$ (*m/z* = 521), $[AuAl_3](Cp^*)_3^+$(*m/z* = 683) and $[HAuAl_4](Cp^*)_4^+$ (*m/z* = 845). Obviously, **3** is quite unstable under the measurement conditions. The LIFDI-MS of isolated **3** shows the presence of trace impurities, these include the larger clusters **1** and **2**, as well as numerous $[Au_x(^i Dipp)_y]^+$ aggregates, which trace impurities are much better ionizable then **3**. The IR spectrum of **3** (see Figure S17) shows the characteristic modes of the Cp* ligand, as well as the Al-Cp* stretching frequency at 455 cm^{-1}. There is no signal of surface bound hydride observed in the spectrum. The UV-Vis spectrum of isolated **3** (see Figure S18) consists of a broad, weak band at 516 nm, a band centered at 417 nm, as well as a broad and intense band at 406 nm. In the UV region, a sharp band at 331 nm is detected. A concentrated solution of **3** in toluene has green-brown color and turns yellow upon dilution. Cluster **3** forms black block-shaped crystallites, which are very air- and moisture sensitive. It crystallizes in the monoclinic space group *P21/n* with four cluster molecules per unit cell and four molecules of co-crystallized toluene (Figure 1). Detailed

crystallographic information is found in Table S1. The structure of **3** consists of a digold-centered trigonal-bipyramidal structure with idealized D_{3h} symmetry. The central axis of **3** slightly deviates from linearity (Al2-Au2-Au1 = 175.1 ° and Al1-Au1-Au2: 174.6 °). The central Au_2 unit (Au1-Au2= 3.881 Å) is surrounded by two terminal AlCp* units and three bridging AlCp* units with obtuse angles between 98.9 ° (Au2-Al5-Au1) and 99.5 ° (Au2-Al3-Au1), spanning an almost equilateral triangle with Al-Al-Al angles ranging from 67.5 to 68.6 °. Au-$AlCp^*_{terminal}$ = 2.397 – 2.420 Å and Au-$AlCp^*_{bridging}$ = 2.537 – 2.585 Å. The Au2-Al2 bond in **3** is with 2.397 Å the shortest molecular Au-Al bond reported so far and well within the sum of the covalent radii of the two elements (2.57 Å).[48] The structure of **3** is comparable with the literature known compounds $[Pd_2(AlCp^*)_5]$, $[M_2(GaCp^*)_5]$ (M= Pd, Pt) and $[Ni_2(AlCp^*)_5]$, but deviation from linearity is more pronounced.[49, 50] The Au-Al distances in **3** (Figure S55) are well comparable to those in the trimetallic cluster $[Ni(AuPPh_3)_6(AuCl)_3(AlCp^*)]$ (2.596(5) Å – 2.633(6) Å)[19] and to the strongly polarized $Au^{\delta-}$-$Al^{\delta+}$ bond (2.402(3) Å) in the complex $[(NON)Al(AuP^tBu_3)]$.[51] Overall, Au-Al bond distances in **3** are slightly shorter than in the solid-state alloy $AuAl_2$ (2.58 Å) as one reference structure.[52] Notably, the Au-Au distance in **3** (Au1-Au2= 3.881 Å) is much longer than in related dimeric molecules or small clusters unambiguously featuring direct, covalent Au-Au bonding.[19, 53, 54]. The interesting bonding situation and electronic relationship to $Ni_2(CO)_5$ and $Ni_2(AlCp^*)_5$ is discussed in a separate publication.[55]

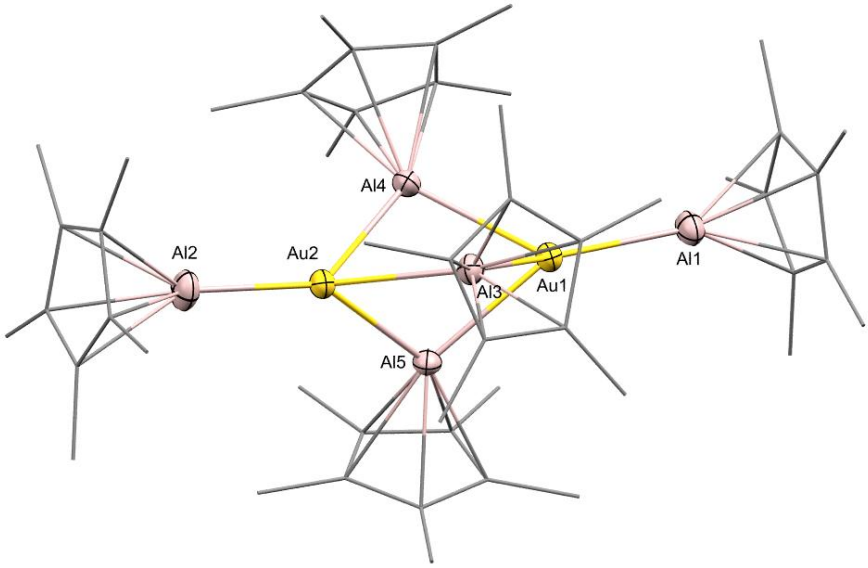

Figure 1: Molecular structure of $[Au_2Al_5](Cp^*)_5$. Au: yellow, Al: pink, C: grey. H-atoms and co-crystallized solvent molecules are omitted and Cp* ligands drawn in wireframe representation for clarity. Thermal ellipsoids are shown at 50% probability level.

The interconnection between larger clusters **1** and **2** and smaller cluster **3** was studied with *in situ* ^{1}H-NMR. The clusters **1** and **2** degrade upon heating in presence of AlCp* and the **3** is formed (see Figure S23 - S25). Treatment of isolated **3** with ^{i}DippAuH (2 eq.) at room temperature results in complete consumption of **3** already after 2.5 h reaction time and the formation of $[Au_6Al_6](Cp^*)_6$ (**1**) (Figure S27).

Conclusion.

Three novel members of intermetalloid Au/Al clusters are prepared and characterized within the scope of this work. The geometric and electronic structures of the larger clusters $[Au_6Al_6](Cp^*)_6$ (**1**) and $[HAu_7Al_6](Cp^*)_6$ (**2**) were investigated through DFT calculations, both clusters can be described as 18 electron superatoms. While SC-XRD of **1** and **2** leads to unsatisfactory results due to heavy disorder in the metal positions, the smaller cluster $[Au_2Al_5](Cp^*)_5$ **(3**) is well characterized by SC-XRD.

The synthesis of the described gold clusters can be controlled using various phosphines as additives. The presence of PPh_3 changes the reduction mechanism of ^{i}DippAuH, which is a key step in the cluster formation: With increasing amount of PPh_3 the reduction by AlCp* is disfavored and the reductive elimination of H_2 becomes dominant. This has remarkable impact on the reaction outcome and the formation of **2** becomes selective.

AUTHOR INFORMATION

Corresponding Author

Roland A. Fischer, roland.fischer@tum.de; Jean-Yves Saillard, jean-yves.saillard@univ-rennes1.fr

Author Contributions

Ivan Antsiburov‡: experimental work, manuscript preparation; Max Schütz‡: experimental work, single crystal X-ray data acquisition and analysis; Christian Gemel: research supervision, manuscript preparation; Raphael Bühler: NMR measurements, manuscript preparation; Maximilian Muhr: initial DFT calculations, manuscript preparation; Johannes Stephan: CIF preparation; Wilhelm Klein: SC-XRD refinement; Samia Kahlal: DFT calculations and theoretical bonding analysis; Jean-Yves Saillard: DFT calculations, theoretical bonding analysis and manuscript preparation; Roland A. Fischer: research conception, manuscript preparation.

Funding Sources

This work was funded by the German Research Foundation (DFG) within a Reinhard Koselleck Project (FI-502/44-1) and supported by the GENCI French National computing resource (grant A0090807367).

REFERENCES

(1) Bellon, P. L.; Cariati, F.; Manassero, M.; Naldini, L.; Sansoni, M. Novel gold clusters. Preparation, properties, and X-ray structure determination of salts of octakis(triarylphosphine)enneagold, [Au9L8]X3. *Journal of the Chemical Society D: Chemical Communications* **1971**, (22), 1423-1424, 10.1039/C29710001423. DOI: 10.1039/C29710001423.
(2) Schmid, G.; Pfeil, R.; Boese, R.; Bandermann, F.; Meyer, S.; Calis, G. H. M.; van der Velden, J. W. A. Au55[P(C6H5)3]12CI6 — ein Goldcluster ungewöhnlicher Größe. *Chemische Berichte* **1981**, *114* (11), 3634-3642, https://doi.org/10.1002/cber.19811141116. DOI: https://doi.org/10.1002/cber.19811141116 (acccessed 2021/07/17).
(3) Briant, C. E.; Theobald, B. R. C.; White, J. W.; Bell, L. K.; Mingos, D. M. P.; Welch, A. J. Synthesis and X-ray structural characterization of the centred icosahedral gold cluster compound [Aul3(PMe2Ph)10Cl2](PF6)3; the realization of a theoretical prediction. *Journal of the Chemical Society, Chemical Communications* **1981**, (5), 201-202, 10.1039/C39810000201. DOI: 10.1039/C39810000201.

(4) Mingos, D. M. P. Structural and bonding patterns in gold clusters. *Dalton Transactions* **2015**, *44* (15), 6680-6695, 10.1039/C5DT00253B. DOI: 10.1039/C5DT00253B.
(5) Vollenbroek, F. A.; Bosman, W. P.; Bour, J. J.; Noordik, J. H.; Beurskens, P. T. Reactions of gold–phosphine cluster compounds. Preparation and X-ray structure determination of octakis(triphenylphosphine)octa-gold bis(hexafluorophosphate). *Journal of the Chemical Society, Chemical Communications* **1979**, (9), 387-388, 10.1039/C39790000387. DOI: 10.1039/C39790000387.
(6) Mingos, D. M. P. Molecular-orbital calculations on cluster compounds of gold. *Journal of the Chemical Society, Dalton Transactions* **1976**, (13), 1163-1169, 10.1039/DT9760001163. DOI: 10.1039/DT9760001163.
(7) Xu, W. W.; Zhu, B.; Zeng, X. C.; Gao, Y. A grand unified model for liganded gold clusters. *Nature Communications* **2016**, *7* (1), 13574. DOI: 10.1038/ncomms13574.
(8) Häkkinen, H. Atomic and electronic structure of gold clusters: understanding flakes, cages and superatoms from simple concepts. *Chemical Society Reviews* **2008**, *37* (9), 1847-1859, 10.1039/B717686B. DOI: 10.1039/B717686B.
(9) Qian, H.; Zhu, M.; Wu, Z.; Jin, R. Quantum Sized Gold Nanoclusters with Atomic Precision. *Accounts of Chemical Research* **2012**, *45* (9), 1470-1479. DOI: 10.1021/ar200331z.
(10) Johnson, G. E.; Laskin, J. Understanding ligand effects in gold clusters using mass spectrometry. *Analyst* **2016**, *141* (12), 3573-3589, 10.1039/C6AN00263C. DOI: 10.1039/C6AN00263C.
(11) Negishi, Y.; Nobusada, K.; Tsukuda, T. Glutathione-Protected Gold Clusters Revisited: Bridging the Gap between Gold(I)−Thiolate Complexes and Thiolate-Protected Gold Nanocrystals. *Journal of the American Chemical Society* **2005**, *127* (14), 5261-5270. DOI: 10.1021/ja042218h.
(12) Daruich De Souza, C.; Ribeiro Nogueira, B.; Rostelato, M. E. C. M. Review of the methodologies used in the synthesis gold nanoparticles by chemical reduction. *Journal of Alloys and Compounds* **2019**, *798*, 714-740. DOI: https://doi.org/10.1016/j.jallcom.2019.05.153.
(13) Ganesamoorthy, C.; Weßing, J.; Kroll, C.; Seidel, R. W.; Gemel, C.; Fischer, R. A. The Intermetalloid Cluster [(Cp*AlCu)6H4], Embedding a Cu6 Core Inside an Octahedral Al6 Shell: Molecular Models of Hume–Rothery Nanophases. *Angewandte Chemie International Edition* **2014**, *53* (30), 7943-7947, https://doi.org/10.1002/anie.201402149. DOI: https://doi.org/10.1002/anie.201402149 (acccessed 2022/03/08).
(14) Weßing, J.; Ganesamoorthy, C.; Kahlal, S.; Marchal, R.; Gemel, C.; Cador, O.; Da Silva, A. C. H.; Da Silva, J. L. F.; Saillard, J.-Y.; Fischer, R. A. The Mackay-Type Cluster [Cu43Al12](Cp*)12: Open-Shell 67-Electron Superatom with Emerging Metal-Like Electronic Structure. *Angewandte Chemie International Edition* **2018**, *57* (44), 14630-14634, https://doi.org/10.1002/anie.201806039. DOI: https://doi.org/10.1002/anie.201806039 (acccessed 2022/03/08).
(15) Schütz, M.; Gemel, C.; Muhr, M.; Jandl, C.; Kahlal, S.; Saillard, J.-Y.; Fischer, R. A. Exploring Cu/Al cluster growth and reactivity: from embryonic building blocks to intermetalloid, open-shell superatoms. *Chemical Science* **2021**, *12* (19), 6588-6599, 10.1039/D1SC00268F. DOI: 10.1039/D1SC00268F.
(16) Fetzer, F.; Schrenk, C.; Pollard, N.; Adeagbo, A.; Clayborne, A. Z.; Schnepf, A. A new reductant in gold cluster chemistry gives a superatomic gold gallium cluster. *Chemical Communications* **2021**, *57* (29), 3551-3554, 10.1039/D0CC07006H. DOI: 10.1039/D0CC07006H.

(17) Pignolet, L. H.; Aubart, M. A.; Craighead, K. L.; Gould, R. A. T.; Krogstad, D. A.; Wiley, J. S. Phosphine-stabilized, platinum-gold and palladium-gold cluster compounds and applications in catalysis. *Coordination Chemistry Reviews* **1995**, *143*, 219-263. DOI: https://doi.org/10.1016/0010-8545(94)07009-9.
(18) Anandhi, U.; Sharp, P. R. A Gallium-Coated Gold Cluster. *Angewandte Chemie International Edition* **2004**, *43* (45), 6128-6131, https://doi.org/10.1002/anie.200461295. DOI: https://doi.org/10.1002/anie.200461295 (acccessed 2021/07/17).
(19) Puls, A.; Jerabek, P.; Kurashige, W.; Förster, M.; Molon, M.; Bollermann, T.; Winter, M.; Gemel, C.; Negishi, Y.; Frenking, G.; et al. A Novel Concept for the Synthesis of Multiply Doped Gold Clusters [(M@AunM′m)Lk]q+. *Angewandte Chemie International Edition* **2014**, *53* (17), 4327-4331, https://doi.org/10.1002/anie.201310436. DOI: https://doi.org/10.1002/anie.201310436 (acccessed 2021/07/17).
(20) Wang, L.; Xu, J.; Kira, M.; Yan, L.; Xiao, X.-Q.; Li, Z. A Stable Cyclic (R2SnAu)3 Anion Having In-Plane σ-Möbius Aromaticity. *Angewandte Chemie International Edition* **2020**, *59* (5), 1980-1984, https://doi.org/10.1002/anie.201910731. DOI: https://doi.org/10.1002/anie.201910731 (acccessed 2021/07/17).
(21) Jadhav, A. P.; Pawar, A.; Kim, C. W.; Cha, H. G.; Pal, U.; Kang, Y. S. Effect of Different Additives on the Size Control and Emission Properties of Y2O3:Eu3+ Nanoparticles Prepared through the Coprecipitation Method. *The Journal of Physical Chemistry C* **2009**, *113* (38), 16652-16657. DOI: 10.1021/jp9059399.
(22) Yin, L.; Wang, Y.; Pang, G.; Koltypin, Y.; Gedanken, A. Sonochemical Synthesis of Cerium Oxide Nanoparticles—Effect of Additives and Quantum Size Effect. *Journal of Colloid and Interface Science* **2002**, *246* (1), 78-84. DOI: https://doi.org/10.1006/jcis.2001.8047.
(23) Rizzuti, A.; Dassisti, M.; Mastrorilli, P.; Sportelli, M. C.; Cioffi, N.; Picca, R. A.; Agostinelli, E.; Varvaro, G.; Caliandro, R. Shape-control by microwave-assisted hydrothermal method for the synthesis of magnetite nanoparticles using organic additives. *Journal of Nanoparticle Research* **2015**, *17* (10), 408. DOI: 10.1007/s11051-015-3213-0.
(24) Yang, Y.; Chen, H.; Zhao, B.; Bao, X. Size Control of ZnO Nanoparticles via Thermal Decomposition of Zinc Acetate Coated on Organic Additives. *Journal of Crystal Growth* **2004**, *263*, 447-453. DOI: 10.1016/j.jcrysgro.2003.12.010.
(25) Heiß, P.; Hornung, J.; Gemel, C.; Fischer, R. A. A combinatorial coordination-modulated approach to all-hydrocarbon-ligated intermetallic clusters. *Chemical Communications* **2022**, 10.1039/D2CC00396A. DOI: 10.1039/D2CC00396A.
(26) Pettibone, J. M.; Hudgens, J. W. Gold Cluster Formation with Phosphine Ligands: Etching as a Size-Selective Synthetic Pathway for Small Clusters? *ACS Nano* **2011**, *5* (4), 2989-3002. DOI: 10.1021/nn200053b.
(27) Ganesamoorthy, C.; Loerke, S.; Gemel, C.; Jerabek, P.; Winter, M.; Frenking, G.; Fischer, R. A. Reductive elimination: a pathway to low-valent aluminium species. *Chemical Communications* **2013**, *49* (28), 2858-2860, 10.1039/C3CC38584A. DOI: 10.1039/C3CC38584A.
(28) Tsui, E. Y.; Müller, P.; Sadighi, J. P. Reactions of a Stable Monomeric Gold(I) Hydride Complex. *Angewandte Chemie International Edition* **2008**, *47* (46), 8937-8940, https://doi.org/10.1002/anie.200803842. DOI: https://doi.org/10.1002/anie.200803842 (acccessed 2021/07/18).
(29) Muhr, M.; Heiß, P.; Schütz, M.; Bühler, R.; Gemel, C.; Linden, M. H.; Linden, H. B.; Fischer, R. A. Enabling LIFDI-MS measurements of highly air sensitive organometallic

compounds: a combined MS/glovebox technique. *Dalton Transactions* **2021**, *50* (26), 9031-9036, 10.1039/D1DT00978H. DOI: 10.1039/D1DT00978H.
(30) Parr, R. G. Density Functional Theory of Atoms and Molecules. In *Horizons of Quantum Chemistry*, Dordrecht, 1980//, 1980; Fukui, K., Pullman, B., Eds.; Springer Netherlands: pp 5-15.
(31) te Velde, G.; Bickelhaupt, F. M.; Baerends, E. J.; Fonseca Guerra, C.; van Gisbergen, S. J. A.; Snijders, J. G.; Ziegler, T. Chemistry with ADF. *Journal of Computational Chemistry* **2001**, *22* (9), 931-967, https://doi.org/10.1002/jcc.1056. DOI: https://doi.org/10.1002/jcc.1056 (acccessed 2022/06/27).
(32) Fonseca Guerra, C.; Snijders, J. G.; te Velde, G.; Baerends, E. J. Towards an order-N DFT method. *Theoretical Chemistry Accounts* **1998**, *99* (6), 391-403. DOI: 10.1007/s002140050353.
(33) ADF2019, S., Theoretical Chemistry, Vrije Universiteit, Amsterdam, The Netherlands, http://www.scm.com. (accessed.
(34) van Lenthe, E.; Baerends, E. J.; Snijders, J. G. Relativistic total energy using regular approximations. *The Journal of Chemical Physics* **1994**, *101* (11), 9783-9792. DOI: 10.1063/1.467943 (acccessed 2022/06/27).
(35) Grimme, S. Semiempirical GGA-type density functional constructed with a long-range dispersion correction. *Journal of Computational Chemistry* **2006**, *27* (15), 1787-1799, https://doi.org/10.1002/jcc.20495. DOI: https://doi.org/10.1002/jcc.20495 (acccessed 2022/06/27).
(36) Van Lenthe, E.; Baerends, E. J. Optimized Slater-type basis sets for the elements 1–118. *Journal of Computational Chemistry* **2003**, *24* (9), 1142-1156, https://doi.org/10.1002/jcc.10255. DOI: https://doi.org/10.1002/jcc.10255 (acccessed 2022/06/27).
(37) Becke, A. D. Density-functional exchange-energy approximation with correct asymptotic behavior. *Physical Review A* **1988**, *38* (6), 3098-3100. DOI: 10.1103/PhysRevA.38.3098.
(38) Perdew, J. P. Density-functional approximation for the correlation energy of the inhomogeneous electron gas. *Physical Review B* **1986**, *33* (12), 8822-8824. DOI: 10.1103/PhysRevB.33.8822.
(39) E.D. Glendening, J. K. B., A.E. Reed, J.E. Carpenter, J.A. Bohmann, C.M. Morales, F. Weinhold, NBO 6.0, Theoretical Chemistry Institute, University of Wisconsin (Madison, WI, 2001, http://nbo6.chem.wisc.edu). . (accessed.
(40) Schreckenbach, G.; Ziegler, T. Calculation of NMR Shielding Tensors Using Gauge-Including Atomic Orbitals and Modern Density Functional Theory. *The Journal of Physical Chemistry* **1995**, *99* (2), 606-611. DOI: 10.1021/j100002a024.
(41) *Gaussian 16 Rev. C.01*; Wallingford, CT, 2016. (accessed.
(42) Perdew, J. P.; Ernzerhof, M.; Burke, K. Rationale for mixing exact exchange with density functional approximations. *The Journal of Chemical Physics* **1996**, *105* (22), 9982-9985. DOI: 10.1063/1.472933 (acccessed 2022/07/13).
(43) Adamo, C.; Barone, V. Toward reliable density functional methods without adjustable parameters: The PBE0 model. *The Journal of Chemical Physics* **1999**, *110* (13), 6158-6170. DOI: 10.1063/1.478522 (acccessed 2022/07/13).
(44) Schäfer, A.; Horn, H.; Ahlrichs, R. Fully optimized contracted Gaussian basis sets for atoms Li to Kr. *The Journal of Chemical Physics* **1992**, *97* (4), 2571-2577. DOI: 10.1063/1.463096 (acccessed 2022/07/13).
(45) Schäfer, A.; Huber, C.; Ahlrichs, R. Fully optimized contracted Gaussian basis sets of triple zeta valence quality for atoms Li to Kr. *The Journal of Chemical Physics* **1994**, *100* (8), 5829-5835. DOI: 10.1063/1.467146 (acccessed 2022/07/13).

(46) Wang, X.; Andrews, L. Gold Is Noble but Gold Hydride Anions Are Stable. *Angewandte Chemie International Edition* **2003**, *42* (42), 5201-5206, https://doi.org/10.1002/anie.200351780. DOI: https://doi.org/10.1002/anie.200351780 (acccessed 2021/07/18).
(47) Luo, Z.; Castleman, A. W. Special and General Superatoms. *Accounts of Chemical Research* **2014**, *47* (10), 2931-2940. DOI: 10.1021/ar5001583.
(48) Cordero, B.; Gómez, V.; Platero-Prats, A. E.; Revés, M.; Echeverría, J.; Cremades, E.; Barragán, F.; Alvarez, S. Covalent radii revisited. *Dalton Transactions* **2008**, (21), 2832-2838, 10.1039/B801115J. DOI: 10.1039/B801115J.
(49) Steinke, T.; Gemel, C.; Winter, M.; Fischer, R. A. The Clusters [Ma (ECp*) b](M= Pd, Pt; E= Al, Ga, In): Structures, Fluxionality, and Ligand Exchange Reactions. *Chemistry–A European Journal* **2005**, *11* (5), 1636-1646.
(50) Hornung, J. Hume-Rothery inspired Complexes and Clusters as Molecular Models for Intermediates in Heterogeneous Catalysis. Technische Universität München, 2019.
(51) Hicks, J.; Mansikkamäki, A.; Vasko, P.; Goicoechea, J. M.; Aldridge, S. A nucleophilic gold complex. *Nature Chemistry* **2019**, *11* (3), 237-241. DOI: 10.1038/s41557-018-0198-1.
(52) Hsu, L.-S.; Wang, Y. K.; Tai, Y. L.; Lee, J. F. Experimental and theoretical study of the electronic structure of $AuAl_2$, $AuGa_2$, and $AuIn_2$. *Physical Review B* **2005**, *72* (11), 115115. DOI: 10.1103/PhysRevB.72.115115.
(53) Gabbai, F. P.; Schier, A.; Riede, J.; Schmidbaur, H. Different Pathways of the Reaction of InCl with Ph3PAuCl: Isolation of the First Mixed-Valent Mixed-Metal Gold/Indium Cluster. *Inorganic Chemistry* **1995**, *34* (15), 3855-3856. DOI: 10.1021/ic00119a003.
(54) Weinberger, D. S.; Melaimi, M.; Moore, C. E.; Rheingold, A. L.; Frenking, G.; Jerabek, P.; Bertrand, G. Isolation of Neutral Mono- and Dinuclear Gold Complexes of Cyclic (Alkyl)(amino)carbenes. *Angewandte Chemie International Edition* **2013**, *52* (34), 8964-8967, https://doi.org/10.1002/anie.201304820. DOI: https://doi.org/10.1002/anie.201304820 (acccessed 2021/07/22).
(55) Hornung, J.; Muhr, M.; Schütz, M.; Heiß, P.; Stephan, J.; Jandl, C.; Gemel, C.; Kahlal, S.; Saillard, J.-Y.; Fischer, R. A. Metal–Metal Bonding in Late Transition-Metal [M2L5] Complexes: Exploring the Limits of the Isolobal Analogy between the CO and AlCp* Ligands. *Inorganic Chemistry* **2023**. DOI: 10.1021/acs.inorgchem.3c00866.